A Letters Journal Exploring the Frontiers of Physics

December 2019

EPL, **128** (2019) 54005 www.epljournal.org
doi: 10.1209/0295-5075/128/54005

Strange nonchaos in self-excited singing flames

D. Premraj[1], Samadhan A. Pawar[1], Lipika Kabiraj[2] and R. I. Sujith[1]

[1] *Indian Institute of Technology Madras - Chennai 600 036, India*
[2] *Indian Institute of Technology Ropar - Rupnagar, Punjab 140 001, India*

received 14 October 2019; accepted in final form 16 December 2019
published online 4 February 2020

PACS 43.28.Kt – Aerothermoacoustics and combustion acoustics
PACS 05.45.-a – Nonlinear dynamics and chaos
PACS 47.10.Fg – Dynamical systems methods

Abstract – We report the first experimental evidence of a strange nonchaotic attractor (SNA) in the natural dynamics of a self-excited laboratory-scale system. In the previous experimental studies, the birth of a SNA was observed in quasiperiodically forced systems; however, such evidence of a SNA in an autonomous laboratory system is yet to be reported. We discover the presence of a SNA between the attractors of quasiperiodicity and chaos through a fractalization route in a laboratory thermoacoustic system. The observed dynamical transitions from order to chaos via a SNA is confirmed through various nonlinear characterization methods prescribed for the detection of a SNA.

Introduction. – Coupled nonlinear systems exhibit various kinds of dynamical behaviours including periodic, quasiperiodic, and chaotic oscillations [1,2]. Among these dynamics, one of the commonly observed states in quasiperiodically driven nonlinear systems is a strange nonchaos. Although strange nonchaotic attractors (SNAs) show similarity to chaotic attractors by having a fractal geometrical structure, SNAs are insensitive to initial conditions unlike the chaotic attractors [3]. Grebogi *et al.* [4] were the first to report the possibility of SNAs in a system of quasiperiodically forced interval maps. Afterwards, several numerical studies have demonstrated the existence of SNAs in quasiperiodically forced systems such as pendulum [5], Duffing oscillator [6], logistic map [7], Henon map [8], and circular map [9].

The experimental discovery of SNA was reported by Ditto *et al.* [10] in a quasiperiodically forced system with a buckled magnetoelastic ribbon. In subsequent years, there have been several experimental observations of SNAs in practical systems [11–15]; however, all these studies presented the necessity of having quasiperiodic forcing to generate SNAs. While these previous investigations on SNA involved external quasiperiodic forcing, Negi *et al.* [16] theoretically showed that quasiperiodic forcing is not essential for the existence of SNA, and it could happen in naturally driven systems as well without the need of external forcing. Recently, Lindner *et al.* [17] showed the observation of SNAs in the natural system of a pulsating star KIC 5520878 network. However, to the best of our knowledge, there has not been a single experimental evidence of SNAs reported in self-driven laboratory systems until now.

Most of the recent studies are focused on identifying the routes to generate SNAs [3,12,18]. The mechanisms for the onset of SNAs are usually classified into three types as: i) Heagy-Hammel route: the SNAs emerges during the collision of a period doubled torus with its own unstable parent [19]. ii) Fractalization route: the truncated torus gets wrinkled and forms SNAs without any interaction with the parent torus [20]. iii) Type-III intermittency route: SNAs occur when the torus doubling bifurcation is controlled by sub-harmonic bifurcations [6]. Another possibility for the occurrence of SNAs is through crisis-induced intermittency, where the collision of the wrinkled torus with the boundary results in sudden widening of the attractor [13].

In this letter, we report the first experimental evidence of SNAs in a self-excited laboratory system, in the absence of external quasiperiodic forcing. We show that the natural dynamics of a laboratory-scale thermoacoustic system [21] displays the presence of SNAs between the quasiperiodic and chaotic attractors.

In a thermoacoustic system, the presence of a flame in a confined environment at certain conditions leads to the generation of a large-amplitude, self-sustained tonal sound in the air column of the system, originally known as "singing flame" [22] or more recently as "thermoacoustic instability" [23]. The occurrence of such self-excited oscillations is detrimental to the structural integrity of

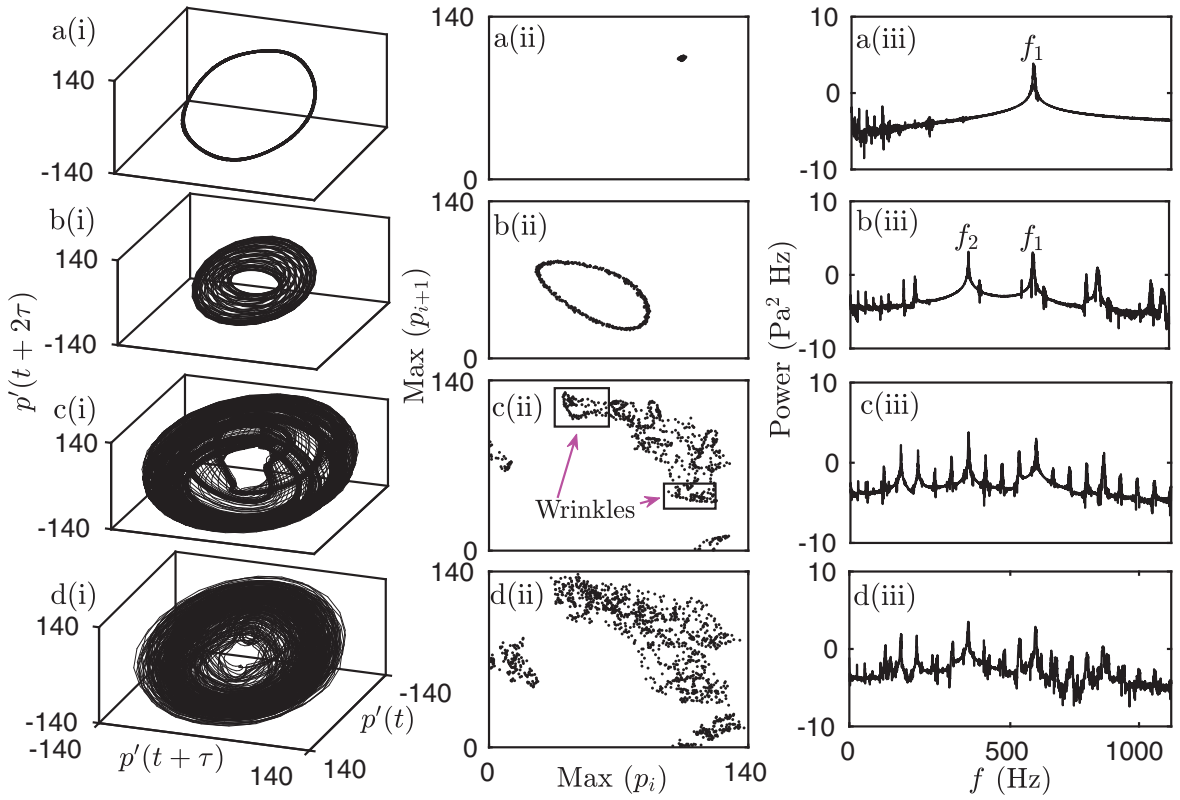

Fig. 1: (a)–(d) The dynamics of acoustic pressure obtained at different $x_f = 0.172$, 0.195, 0.22, and 0.226 for the states of limit cycle, quasiperiodicity, strange nonchaos, and chaos, respectively. For each state, (i) the phase portrait, (ii) Poincaré section, and (iii) power spectrum are plotted. A data set with 10000 points (approximately 570 cycles of oscillations) was considered for obtaining the plots. The number of cycles corresponds to the frequency peak at 569.9 Hz.

practical combustion systems used in propulsion and power generating units [24,25]. Through the implementation of various time series analysis techniques based on the Fourier amplitude spectrum, singular continuous spectrum, correlation dimension, and 0-1 test, we confirm the presence of SNAs in our system.

Experimental details. – The experiments were performed on a laboratory-scale ducted laminar premixed flame combustor. More details on the description of the experimental setup, data acquisition, and measurement uncertainties can be found in Kabiraj *et al.* [21]. The combustor comprises a transparent borosilicate glass duct of inner diameter 5.67 cm and length 80 cm. The glass duct is closed at the bottom end and open at the top end. It consists of a burner tube of length 80 cm, inner diameter 1.6 cm, and thickness 0.15 cm, which is used to supply the premixed air and fuel (Liquefied Petroleum Gas) mixture required for combustion. A circular copper block of 1.8 cm height, with seven 0.2 cm size through holes, is fixed over the burner tube to stabilize the conical flames in the combustor. The equivalence ratio is fixed at 0.48 throughout the study. The combustion mixture is ignited from the top of the burner tube using a butane torch until all flames are stabilized on the copper block.

The location of these flames with respect to the open end of the glass duct (L_f) is varied as a control parameter in this study. We normalize L_f with the length of the duct (L) as $x_f = L_f/L$, where $L = 80$ cm. The dynamics of the combustor for a given change in x_f is acquired in terms of acoustic pressure measurements, performed using a pressure transducer (PCB 103B02 of sensitivity = 223.4 mV/kPa and uncertainty = ±0.14 Pa) located 5 cm from the bottom of the glass duct. The data are acquired using an analog to digital conversion card (NI-6143, 16-bit, resolution = 0.15 mV, voltage range = ±5 V). The data were acquired for 30 s at the sampling frequency of 10 kHz. The frequency resolution of the amplitude spectrum is 0.03 Hz.

Results and discussion. – Primarily, to understand the dynamical transitions of the considered system and to distinguish each dynamical behavior, we plot the reconstructed phase portrait (figs. 1(a)–(d)(i)) of the acoustic pressure signal (p') using a delay embedding theorem proposed by Takes [26]. The time delayed vectors are constructed as follows:

$$P(t) = [p'(t), p'(t+\tau), p'(t+2\tau), \ldots, p'(t+(m-1)\tau)],$$

where $t = 1, \ldots, [N-(m-1)\tau]$, τ is the optimum time delay obtained from the average mutual information and m is the embedding dimension obtained from the method of the false nearest neighbor [27]. Figures 1(a)–(d)(ii) show the Poincaré sections corresponding to the phase

portraits shown in figs. 1(a)–(d)(i). We use here a method based on the first return map to plot the Poincaré section of the p' signal [26]. In this method, we calculate the local positive maxima of every oscillation cycle in the pressure signal and plot the local maxima (p_i) of one oscillation cycle with respect to the local maxima (p_{i+1}) of the next oscillation cycle as a Poincaré section. We also plot the power spectrums of each p' signal in figs. 1(a)–(d)(iii). With the variation x_f, we show that the system behaviour exhibits a transition from limit cycle oscillations to chaotic oscillations via quasiperiodicity and SNAs (see figs. 1(a)–(d), respectively). When x_f is at $= 0.172$, we notice the occurrence of a limit cycle attractor (fig. 1(a)). During this state, the system dynamics evolves on a single periodic orbit in the phase portrait (fig. 1a(i)) and shows an isolated point in the Poincaré section (fig. 1(a)(ii)). Further, the presence of a single dominant frequency peak at $f_1 = 569.9$ Hz in the power spectrum affirms the presence of a limit cycle attractor (see fig. 1(a)(iii)).

For $x_f = 0.195$, we notice the existence of quasiperiodic oscillations as a consequence of the interplay between incommensurate frequencies $f_1 = 569.9$ Hz and $f_2 = 370.5$ Hz, and the peaks at their linear combinations in the power spectrum (see fig. 1(b)(iii)). The reconstructed phase space of a quasiperiodic attractor shows a 2-torus structure and a closed loop of points in the Poincaré section (figs. 1(b)(i) and (b)(ii), respectively).

By changing the flame location to $x_f = 0.22$, we find that the stable 2-torus attractor observed for quasiperiodic oscillations (fig. 1(b)(i)) wrinkles and fractalizes (fig. 1(c)(i)), we identify the resulting attractor as a SNA in subsequent analysis (description of figs. 2–4). This fractalization of the attractor can be seen from the Poincaré sections of these attractors, where a closed loop structure of the quasiperiodic attractor (fig. 1(b)(ii)) breaks down into a wrinkled torus structure of SNA (fig. 1c(ii)). As the SNA emerges from a quasiperiodic attractor and is followed by chaos, the appearance of a SNA conforms to the *fractalization* route [20] in the system dynamics. The dynamical mechanism behind this route involves the destabilization and fractalization of the orbits on the torus without colliding with its parent unstable torus during the transition to the SNA (compare figs. 1(b)(i) and c(i)). In addition, the power spectrum in fig. 1(c)(iii) for the SNA depicts the presence of several peaks at irrational frequencies with respect to the frequency peak f_1, as compared to the case of the quasiperiodic oscillations.

For $x_f = 0.226$, the acoustic pressure exhibits aperiodic fluctuations, which occur when the unstable periodic orbits on the SNAs get more destabilized and wrinkled to form a chaotic attractor, as seen from fig. 1(d)(i). The Poincaré section of this state shows a scatter of points on its surface (fig. 1(d)(ii)) and the power spectrum indicates a broadband behaviour (fig. 1(d)(iii)), confirming the presence of chaotic dynamics in the signal.

In the subsequent portion of the paper, we use various tools to qualitatively and quantitatively characterize the dynamics of different dynamical states and also reaffirm the existence of SNAs in our system.

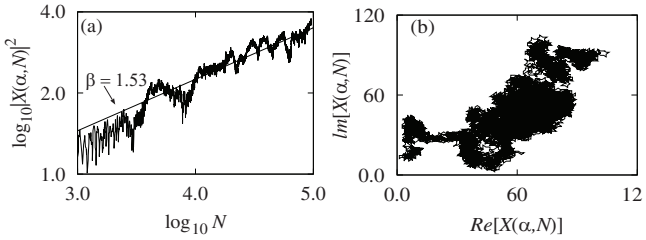

Fig. 2: Singular continuous spectrum analysis of pressure signal obtained at $x_f = 0.22$. (a) The logarithmic plot of $|X(\alpha, N)|^2$ against N shows the power law scaling, and (b) the fractal path in the complex plane of X confirms the presence of SNAs. α corresponds to the dominant frequency observed at 569.9 Hz in fig. 1(c)(iii).

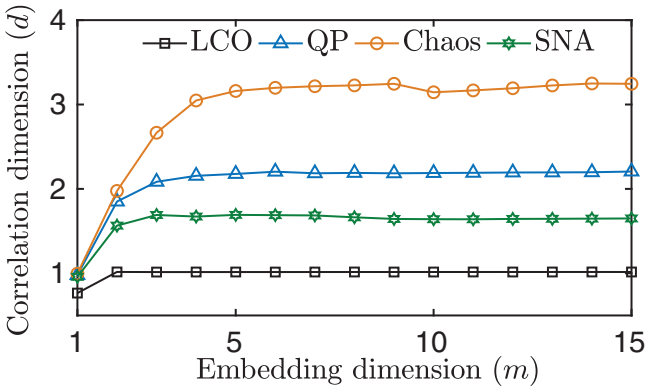

Fig. 3: Variation of correlation dimension (d) with embedding dimension (m) for the states limit cycle (LCO), quasiperiodicity (QP), strange nonchaos (SNA), and chaos, as shown in fig. 1.

Singular continuous spectrum. – In general, a dynamical system can manifest two types of power spectrum, namely, continuous and discrete spectrum [28]. The discrete spectrum corresponds to the occurrence of oscillations at specific frequencies, similarly to what is observed for the periodic or quasiperiodic oscillations.

In contrast, the broadband nature of the power spectrum observed for the case of chaotic oscillations points towards the presence of continuous spectrum. For a special case like SNA, the spectrum exhibits a combination of both continuous and discrete components, known as singular continuous spectrum [28–31]. The singular continuous spectrum is defined based on the Fourier transform of a signal x_k as

$$X(\alpha, N) = \sum_{k=1}^{N} (x_k) \exp(2\pi i k \alpha), \qquad (1)$$

where α corresponds to the frequency and N indicates time. Since $X(\alpha, N)$ is a complex variable, the plot between $\mathrm{Re}(X)$ and $\mathrm{Im}(X)$ helps us understand different

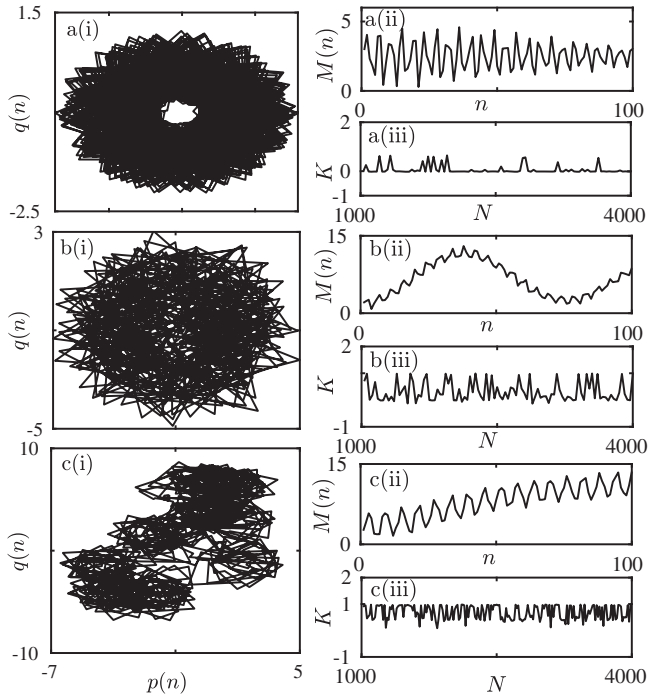

Fig. 4: A 0-1 test performed to distinguish the dynamics of (a) quasiperiodicity at $x_f = 0.172$, (b) strange nonchaos at $x_f = 0.22$, and (c) chaos at $x_f = 0.226$. (i) The plot between the translation variables $p(n)$ and $q(n)$, (ii) the behaviour of mean square displacement $M(n)$ with n, and (iii) the variation of the growth rate K for these dynamical states are shown.

dynamical features exhibited by the signal. For regular (periodic and quasiperiodic) signals as the spectrum is discrete, the power $|X(\alpha, N)|^2$ is proportional to N^2 and a path on the $[\mathrm{Re}(X), \mathrm{Im}(X)]$-plane displays a persistent and bounded behaviour [28]. If the path in the complex plane is random (Brownian walk), then the power of the signal $|X(\alpha, N)|^2$ is directly proportional to N, denoting the continuous spectral components observed for chaotic signals. For the singular continuous spectrum, the power $|X(\alpha, N)|^2$ is proportional to N^β and the value of β lies between 1 and 2 [28]. For the state of acoustic pressure fluctuations observed at $x_f = 0.22$ (fig. 1(c)), we notice the value of $\beta = 1.53$ such that $1 < \beta < 2$ (fig. 2(a)) and the trajectory path on the $[\mathrm{Re}(X), \mathrm{Im}(X)]$-plane displays a self-similar fractal structure (fig. 2(b) and figs. 1 and 2 of the Supplementary Material `Supplementarymaterial.pdf` (SM). Thus, we confirm the presence of SNA in the pressure oscillations observed at this x_f. The singular continuous spectrum analysis for quasiperiodic and chaotic oscillations is provided in fig. 3 of the SM.

Correlation dimension. – In order to differentiate the regular and the strange behaviour of attractors demonstrated in fig. 1, we estimate the correlation dimension for each dynamical state, as shown in fig. 3. We follow the algorithm of Grassberger and Procacia [32,33] to calculate the correlation dimension. In this method, we first need to reconstruct the experimental signal in its embedded phase space as discussed in the previous section. The correlation dimension d of an attractor is then obtained as follows:

$$d = \lim_{r \to 0} \frac{\ln C(\epsilon)}{\ln \epsilon}, \tag{2}$$

where ϵ is the distance threshold used to count the nearest neighbors of any state point on the attractor and $C(\epsilon)$ is the correlation sum which is identified using the following relation:

$$C(\epsilon) = \lim_{N \to \infty} \frac{1}{N} \sum_{i,j=1}^{N} \Theta(\epsilon - ||x_i - x_j||), \tag{3}$$

where Θ is the Heaviside function. If the distance ϵ is positive, then $\Theta(\epsilon) = 1$; else $\Theta(\epsilon) = 0$. x_i and x_j are the state vectors. The value of $C(\epsilon)$ is dependent on the value of ϵ and obeys the power-law for a certain range of ϵ such that, $C(\epsilon) = \epsilon^d$ (details are available in the SM).

The correlation dimension attains an integer value for regular attractor (periodic and quasiperiodic), whereas it shows a non-integer value for the strange attractor (chaos and SNA). For the limit cycle attractor, the value of d is near 1, whereas for the quasiperiodic attractor, d takes a value near 2 [34]. In order to confirm the dynamical behaviour of signals shown in fig. 1, we plot the correlation dimension (d) as a function of the embedding dimension (m) [32–34] in fig. 3. The value of d at which its variation with m saturates is considered as the correlation dimension of the particular attractor. We observe that for limit cycle oscillation (LCO), the correlation dimension saturates near 1.01 ± 0. On the other hand, for the quasiperiodic oscillations, the value of d saturates near 2.19 ± 0.02, which is close to the value of 2 predicted theoretically for this attractor [34]. For SNA and chaos, the value of d is observed to be 1.66 ± 0.02 and 3.19 ± 0.06, respectively. These non-integer values of d further confirm the strange geometry of these attractors.

0-1 test. – Furthermore, the usual practice to distinguish the aforementioned dynamical states is to calculate the maximum Lyapunov exponent of the signal, whose value is positive for a chaotic signal and negative for SNA [35]. However, as most of the experimental data contain intrinsic noise, the computation of the maximum Lyapunov exponent gets challenging. Hence, confirming the chaos or SNA in the system dynamics using Lyapunov exponent becomes unfeasible [2]. Therefore, in order to distinguish the dynamics of SNA from chaos, we make use of the 0-1 test [36], as suggested by Gopal *et al.* [37].

The first step in implementing the 0-1 test is to compute the translation variables, denoted as $p(n)$ and $q(n)$, from the input time series $\phi(j)$ such that [36]

$$p(n) = \sum_{j=1}^{n} \phi(j) \cos(jc)$$

and

$$q(n) = \sum_{j=1}^{n} \phi(j) \sin(jc). \tag{4}$$

Here, $n = 1, 2, \ldots, N$. The value of the constant c can be chosen in the interval $(\pi/5, 4\pi/5)$. The behaviour of these two new variables helps in distinguishing different dynamical states in the system. For regular dynamics (periodic or quasiperiodic), the behaviour of these variables is bounded, while it is unbounded or drifting for chaotic dynamics. The motion of translation variables depends on the value of n, which is much less than N and often chosen as $n = N/10$ [36]. The behaviour of the trajectory in the $[p(n), q(n)]$-plane for increasing n can be calculated through the mean square displacement $D(n)$ as follows:

$$D(n) = \frac{1}{N} \sum_{j=1}^{n} ([p(j+n) - p(j)]^2 + [q(j+n) - q(j)]^2).$$

In order to resolve convergence issues of $D(n)$, a modified mean square displacement is used [36,38], which is obtained as follows:

$$M(n) = D(n) - V_{osc}(c, n),$$

where $V_{osc}(c, n) = \frac{1}{N} \sum_{j=1}^{n} \phi(j) \frac{(1-\cos(jc))}{(1-\cos(c))}$. For a chaotic signal, the value of $M(n)$ will linearly increase with n, whereas for a regular signal, it remains nearly constant [36,38]. Further, the asymptotic growth rate of such mean displacements is calculated through a linear regression, which is given by the following equation:

$$K = \lim_{n \to \infty} \frac{\log M(n)}{\log n}. \tag{5}$$

The value of K lies between 0 and 1 [39]. If the dynamics are chaotic, K takes a value close to 1, and for a regular signal, it approaches 0. In order to distinguish the dynamics of SNA from regular and chaotic oscillations, Gopal *et al.* [37] suggested that the choice of c should be the Golden mean ratio, *i.e.*, $c = (\sqrt{5} + 1)/2$. For SNAs, the value of K lies between 0 and 1.

In figs. 4(a)-(c), we plot the translation variable $p(n)$ *vs.* $q(n)$ for the dynamics of quasiperiodic, SNA, and chaotic oscillations, respectively. The trajectory in the (p, q)-plane appears to be bounded along a circle, indicative of quasiperiodic dynamics (fig. 4(a)) in the pressure signal obtained at $x_f = 0.172$. Furthermore, the mean displacement $M(n)$ exhibits fluctuations around some constant value (fig. 4(a)(ii)) and the growth rate shows a value near zero (fig. 4(a)(iii)), confirming the quasiperiodic dynamics [37] of the pressure oscillation observed during this state. On the other hand, for the chaotic signal (fig. 4(c)(i)), the trajectory in the (p, q)-plane shows a random-walk (or Brownian) type behaviour. The variation of $M(n)$ with n displays an increasing trend (fig. 4c(ii)) with a growth value (K) near unity (fig. 4c(iii)), further affirming the presence of chaotic oscillations in the pressure signal obtained at $x_f = 0.226$. Since SNA consists of properties of both regular and chaotic dynamics, we notice the presence of bounded trajectory with a minimal Brownian structure [37] in the (p, q)-plane (fig. 4b(i)). The presence of SNAs can also be confirmed from the plot of variation of $M(n)$ with n, where the mean of this plot does not increase monotonically but shows an oscillatory behaviour with n, along with the value of K lying between 0 and 1 [36,38]. Thus, using the 0-1 test, we distinguish the features of SNA from quasiperiodic and chaotic dynamics in our system.

Conclusions. – We report the first experimental evidence of SNAs in the natural dynamics of a laboratory-system which is not quasiperiodically forced. This observation is in contrast with the usual experimental studies on SNAs that requires quasiperiodic forcing for the birth of SNAs. We witness the existence of SNAs between the states of quasiperiodic and chaotic dynamics in a laminar thermoacoustic system when the flame location in the combustor is varied as the control parameter. The presence of a SNAs is confirmed through methods such as singular-continuous spectrum, correlation dimension, and 0-1 test. The birth of SNAs is shown to happen via fractalization route. The experimental evidence of SNAs would be a benchmark for models that are developed to capture the quasi-periodicity route to chaos observed in experiments.

In general, as the observation of SNAs occurs only in a narrow interval of control parameter between quasiperiodicity and chaos, the detection of such attractors through experiments is difficult. The presence of SNA in the system dynamics has been projected to have wide applications including secure communication, ease of synchronization, and computation process [3]. However, the implementation of SNAs in real-time applications is still a topic of investigation. The experimental realization of SNAs in self-excited dynamics of a laboratory system is a first step in realizing the possibility of such dynamics in practical systems without any forcing. We believe that the existence of SNAs is more ubiquitous in self-excited systems than previously thought.

* * *

We gratefully acknowledge the J. C. Bose fellowship (JCB/2018/000034/SSC) and Swarnajayanti fellowship (DST/SF/1(EC)/2006) from the Department of Science and Technology (DST), Government of India for the financial support.

REFERENCES

[1] Lakshmanan M. and Rajasekar S., *Nonlinear Dynamics: Integrability, Chaos and Patterns* (Springer-Verlag, Berlin) 2003.

[2] Feudel U., Kuznetsov S. and Pikovsky A., *Strange Nonchaotic Attractors: Dynamics Between Order and Chaos in Quasiperiodically Forced Systems* (World Scientific, Singapore) 2006.

[3] Prasad A., Negi S. S. and Ramaswamy R., *Int. J. Bifurc. Chaos*, **11** (2001) 291.

[4] Grebogi C., Ott E., Pelikan S. and Yorke J. A., *Physica D*, **13** (1984) 261.

[5] Romeiras F. J. and Ott E., *Phys. Rev. A*, **35** (1987) 4404.

[6] Venkatesan A., Lakshmanan M., Prasad A. and Ramaswamy R., *Phys. Rev. E*, **61** (2000) 3641.

[7] Prasad A., Mehra V. and Ramaswamy R., *Phys. Rev. E*, **57** (1998) 1576.

[8] Al-Shameri W. F. H., *Int. J. Math. Anal.*, **6** (2012) 2419.

[9] Jäger T., *Commun. Math. Phys.*, **289** (2009) 253.

[10] Ditto W. L., Spano M. L., Savage H. T., Rauseo S. N., Heagy J. and Ott E., *Phys. Rev. Lett.*, **65** (1990) 533.

[11] Guan Y., Meenatchidevi M. and Larry L. K. B., *Chaos*, **28** (2018) 093109.

[12] Thamilmaran K., Senthilkumar D. V., Venkatesan A. and Lakshmanan M., *Phys. Rev. E*, **74** (2006) 036205.

[13] Venkatesan A., Murali K. and Lakshmanan K., *Phys. Lett. A*, **259** (1999) 246.

[14] Premraj D., Suresh K., Palanivel J. and Thamilmaran K., *Commun. Nonlinear Sci. Numer. Simul.*, **50** (2017) 103.

[15] Asir M. P., Murali K. and Philominathan P., *Chaos Solitons Fractals*, **118** (2019) 83.

[16] Negi S. S. and Ramaswamy R., *J. Pramana*, **56** (2001) 47.

[17] Lindner J. F., Kohar V., Kia B., Hippke M., Learned J. G. and Ditto W. L., *Phys. Rev. Lett.*, **114** (2015) 054101.

[18] Venkatesan A. and Lakshmanan M., *Phys. Rev. E*, **63** (2001) 026219.

[19] Heagy J. F. and Hammel S. M., *Physica D*, **70** (1994) 140.

[20] Nishikawa T. and Kaneko K., *Phys. Rev. E*, **54** (1996) 6114.

[21] Kabiraj L., Saurabh A., Wahi P. and Sujith R. I., *Chaos*, **22** (2012) 023129.

[22] Jones A. T., *J. Acoust. Soc. Am.*, **16** (1945) 254.

[23] Matthew J. P. and Sujith R. I., *Annu. Rev. Fluid Mech.*, **50** (2018) 661.

[24] Lieuwen T. C. and Yang V., *Combustion Instabilities in Gas Turbine Engines: Operational Experience, Fundamental Mechanisms, and Modeling,* in *Progress in Astronautics and Aeronautics*, Vol. **210** (AIAA, Inc.) 2005.

[25] Putnam A., *Combustion-Driven Oscillations in Industry* (Elsevier Publishing Company) 1971.

[26] Nayfeh A. H. and Balachandran R., *Applied Nonlinear Dynamics: Analytical, Computational, and Experimental Methods* (Wiley-VCH, Weinheim) 2004.

[27] Abarbanel H., *Analysis of Observed Chaotic Data* (Springer Science & Business Media) 2012.

[28] Pikovsky A. S. and Feudel U., *J. Phys. A*, **27** (1994) 5209.

[29] Yalcinkaya T. and Lai Y. C., *Phys. Rev. E*, **56** (1997) 1623.

[30] Eckmann J. P., Kamphorst S. O. and Ruelle D., *Europhys. Lett.*, **4** (1987) 973.

[31] Pikovsky A. S., Zaks M. A., Feudel U. and Kurths J., *Phys. Rev. E*, **52** (1995) 285.

[32] Grassberger P. and Procaccia I., *Phys. Rev. Lett.*, **50** (1983) 346.

[33] Grassberger P. and Procaccia I., *Physica D*, **9** (1983) 189.

[34] McMahon C. J., Toomey J. P. and Kane D. M., *PLoS One*, **12** (2017) ee0181559.

[35] Kantz H. and Schreiber T., *Nonlinear Time Series Analysis* (Cambridge University Press, Cambridge) 1997.

[36] Gottwald G. A. and Melbourne I., *Proc. R. Soc. London A*, **460** (2004) 603.

[37] Gopal R., Venkatesan A. and Lakshmanan M., *Chaos*, **23** (2013) 023123.

[38] Gottwald G. A. and Melbourne I., *SIAM J. Appl. Dyn. Syst.*, **8** (2009) 129.

[39] Ashwin P., Melbourne I. and Nicol M., *Physica D*, **14** (2001) 275.